scientific reports

Check for updates

OPEN

Unveiling a new oceanic anoxic event at the Norian/Rhaetian boundary (Late Triassic)

Manuel Rigo[1,2]✉, Xin Jin[3], Linda Godfrey[4], Miriam E. Katz[4,5], Honami Sato[6], Yuki Tomimatsu[6,13], Mariachiara Zaffani[1], Matteo Maron[7], Sara Satolli[7], Giuseppe Concheri[8], Alessandra Cardinali[8], Qiangwang Wu[1], Yixing Du[3], Jerry Zhen Xiao Lei[9], Connor S. van Wieren[9], Lydia S. Tackett[10], Hamish Campbell[11], Angela Bertinelli[12] & Tetsuji Onoue[6]

The latest Triassic was characterised by protracted biotic extinctions concluding in the End-Triassic Extinction (~ 200 Ma) and a global carbon cycle perturbation. The onset of declining diversity is closely related to reducing conditions that spread globally from upper Sevatian (uppermost Norian) to across the Norian-Rhaetian boundary, likely triggered by unusually high volcanic activity. We correlate significant organic carbon cycle perturbations to an increase of CO_2 in the ocean–atmosphere system, likely outgassed by the Angayucham igneous province, the onset of which is indicated by the initiation of a rapid decline in $^{87}Sr/^{86}Sr$ and $^{188}Os/^{187}Os$ seawater values. A possible causal mechanism involves elevated CO_2 levels causing global warming and accelerating chemical weathering, which increased nutrient discharge to the oceans and greatly increased biological productivity. Higher export production and oxidation of organic matter led to a global O_2 decrease in marine water across the Norian/Rhaetian boundary (NRB). Biotic consequences of dysoxia/anoxia include worldwide extinctions in some fossil groups, such as bivalves, ammonoids, conodonts, radiolarians.

Dramatic middle and late Mesozoic climate events are often associated with significant spread of reducing conditions and linked to increases in extinction rates[1,2]. These discrete episodes are characterised by intense perturbations in the global carbon cycle that typically record low O_2 conditions and widespread changes in ocean chemistry, called Oceanic Anoxic Events (OAEs)[2–5]. The OAEs are conventionally described as being characterized by black and dark shales with fine laminations and absence of bioturbation, increased sedimentary organic matter and presence of pyrite crystals that attest to low-oxygen conditions[2]. However, the black shale record is sometimes limited in some OAEs or even absent, as occurred for the Paleocene-Eocene Thermal Maximum (PETM)[5,6]. In addition to these sedimentological markers, concentrations and isotopes of several chemical species (e.g., Mo, V, U) are largely applied as redox indicators to identify the OAEs[1,5]. Most OAEs also are characterized by an initial negative $\delta^{13}C$ excursion (CIE) due to input of light carbon (^{12}C) into the ocean–atmosphere system, followed by a positive CIE due to burial of excess ^{12}C in organic-rich sediments[1,5,7]. Notably, the position of the CIEs related to OAEs can vary locally when compared to the deposition of the

[1]Department of Geosciences, University of Padova, Via G. Gradenigo 6, 35131 Padova, Italy. [2]IGG-CNR (Istituto Di Geoscienze E Georisorse), Padova, Firenze, Italy. [3]State Key Laboratory of Oil and Gas Reservoir Geology and Exploitation and Key Laboratory of Deep-Time Geography and Environment Reconstruction and Applications of Ministry of Natural Resources, Chengdu University of Technology, Chengdu 610059, China. [4]Department Earth and Planetary Sciences Rutgers, The State University of New Jersey, Piscataway, NJ 08854-8066, USA. [5]Geosciences Dept, Union College, Schenectady, NY 12308, USA. [6]Department of Earth and Planetary Sciences, Kyushu University, Fukuoka 819-0395, Japan. [7]Department of Engineering and Geology, University "G. d'Annunzio" of Chieti-Pescara, Via Dei Vestini 31, 66100 Chieti, Italy. [8]Department of Agronomy Food Natural Resources Animals and Environment (DAFNAE), University of Padova, Viale Dell'Università, 16, 35020 Legnaro, Italy. [9]School of Earth and Ocean Sciences, University of Victoria, 3800 Finnerty Road, Bob Wright Centre A405. Victoria, Victoria, British Columbia V8P 5C2, Canada. [10]Department of Geological Sciences, Geological Sciences Bldg, University of Missouri, 101, 400 S 6Th St, Columbia, MO 65201, USA. [11]GNS Science, 1 Fairway Drive, 5010 Lower Hutt, Wellington, New Zealand. [12]Departmento of Physics and Geology, University of Perugia, Via A. Pascoli, 06123 Perugia, Italy. [13]Department of Earth System Science, Fukuoka University, Fukuoka 814-0180, Japan. ✉email: manuel.rigo@unipd.it

dark to black shales, indicating that the oceanic oxygen depletion events are diachronous across sedimentary basins [1]. Furthermore, OAEs are generally related to sea water warming indicated by low $\delta^{18}O$ values, which is however commonly interrupted by cooling phases likely caused by the increase of organic matter burial and pCO_2 decrease[1,5].

Phanerozoic OAEs are defined by intervals of widespread oxygen depletion in the ocean, recognized by sedimentological and/or geochemical records, yet they are significantly dissimilar from each other[5]. Jurassic and Cretaceous OAEs are particularly well-studied, such as the early Toarcian (*Posidonienschiefer* event, T-OAE, ~ 183 Ma), early Aptian (Selli event, OAE 1a, ~ 120 Ma), early Albian (Paquier event, OAE 1b, ~ 111 Ma) and Cenomanian–Turonian (Bonarelli event, OAE 2, ~ 94 Ma) events[1,8]. Potential forcing mechanisms for OAEs include massive releases of methane (CH_4) or volcanogenic carbon dioxide (CO_2) outgassing into the atmosphere during the emplacement of Large Igneous Provinces (LIPs) as continental flood basalts or oceanic plateaus[1,9]. For example, OAE 1a correlates to the Ontong Java Plateau, OAE 2 is associated with the Caribbean-Colombian Plateau[1] and the early Toarcian OAE is linked to the Karoo–Ferrar subaerial flood basalt extrusions[10]. Similar scenarios occurred during the late Sevatian (late Norian, Late Triassic) and across the Norian-Rhaetian boundary (NRB), during which significant biotic extinctions of important terrestrial and marine taxa occurred[11]. Notably, cosmopolitan bivalves (e.g., monotids, halobiids) are one of the major fossil groups that suffered a global and severe extinction, starting from the Sevatian to the lowermost Rhaetian[11–13], while ammonoids suffered the largest decline among invertebrates, with a reduction in genera by more than an order of magnitude[14,15]. Other faunal extinctions and diversity loss also are documented for radiolarians and conodonts[16–18], marine vertebrates (e.g., actinopterygian fishes) and reptiles (particularly among ichthyosaurs)[19]. In addition, reef communities declined significantly during the Late Triassic[20]. This interval of strong faunal extinctions at the NRB is associated with large carbon isotope excursions recorded on land[21,22] and in marine environments[11], which are linked to oscillations of biological pump efficiency and/or ocean stratification[11].

We investigated and compared redox conditions recorded in several NRB sections deposited in different sedimentary environments (from shallow to deep water) on opposite sides of Pangea, spanning both hemispheres and across latitudes (Fig. 1). The Pignola-Abriola and Sasso di Castalda sections were deposited in the deep pelagic Lagonegro Basin (Italy), which was part of the western Tethys[23,24]. The Lagonegro Basin records the change from carbonate to biosiliceous sedimentation below the carbonate compensation depth (CCD) across the NRB[25–27]. Both these sections were previously investigated for bio- and chemostratigraphy[11,23–25,27–34], while magnetostratigraphy was performed only in Pignola-Abriola section[35]. The southern Tethys Wombat Basin (NW Australia) was a neritic continental shelf environment located in the southern Tethys on the margin of Pangea, and was recently studied for biostratigraphy[36] and chemostratigraphy[11]. The Kiritehere section (New Zealand) was deposited from mid-shelf to deeper water basin on the southernmost margin of Gondwana, close to the South Pole, and it has been recently investigated for organic carbon[37]. The Holberg section (British Columbia, Canada) is illustrated here for the first time and it represents a shallow to moderate depth depositional environment off an oceanic plateau in eastern Panthalassa, and it has been studied for organic carbon stable isotopes ($\delta^{13}C_{org}$) and chemostratigraphy (this study; Supplementary material). The Katsuyama section (Japan) was deposited below the CCD in the north Equatorial belt of the Panthalassa Ocean has been studied for bio- and chemostratigraphy and $\delta^{13}C_{org}$ (this study; Supplementary material). All these sections spanned the uppermost Sevatian to lower Rhaetian, which is usually characterized by laminated layers and dark to black shales, except for the Katsuyama section that consists of red and dark red shales and cherts([11] and Supplementary material). Notably, the Kiritehere section mostly consists of dark volcanoclastic rocks without any particularly darker portions of the succession. The NRB is identified with the first occurrence of the conodont *Misikella posthernsteini* or (when necessary) is approximated by the negative $\delta^{13}C_{org}$ peak just below the base of the Rhaetian[11,24]. The Wombat and Holberg sections and the Calcari con Selce Formation in the Pignola-Abriola and Sasso di Castalda sections are cherty limestones.

Geochemical evidence of redox conditions at the NRB

Geochemical proxies are used to reconstruct oceanic redox conditions (e.g., V, U, and Mo enrichment)[8,38–43]. Enrichment factors (expressed as X_{EF}, see Methods in Supplementary material) for Cr, V, U, and Mo have been widely used to characterize marine redox conditions [e.g[38,44–46]], which generally can be classified as oxic, suboxic, anoxic, or euxinic (presence of free H_2S)[47]. In this study, these redox-sensitive elements were used to investigate redox conditions across different regions and depths.

Higher concentrations of elements that indicate suboxic to anoxic environments (Cr, V, U, and Mo) were observed in the NRB of the Tethys and eastern Panthalassa oceans (Fig. 1). A slight enrichment of Cr in the Wombat section suggests that at least suboxic conditions existed in the southeastern Tethys Ocean during the NRB interval. Across the NRB, a significant increase in V_{EF} is recorded in sediments deposited in intermediate to deep water environments, represented by the Holberg, Pignola-Abriola and Sasso di Castalda sections (Fig. 1). Vanadium reduction occurs under lower oxygen concentrations[45]. In oxic seawater, V is present as soluble V(V) in the quasi-conservative form of vanadate oxyanions (HVO_4^{2-} and $H_2VO_4^{2-}$). When conditions change from suboxic to weakly anoxic, V(V) converts to V(IV) and forms the vanadyl ion (VO^{2+}), related hydroxyl species ($VO(OH)^{3-}$), and insoluble hydroxides ($VO(OH)_2$)[48,49]. The highest concentration of V is recorded in the NRB of the Pignola-Abriola section, where V_{EF} values are relatively constant and close to the value of 1 in the Sevatian and abruptly increase across the NRB (Fig. 1). Similar V enrichments are found in the NRB of the Holberg and Sasso di Castalda sections. In the Wombat section, V increases across the NRB, indicating that the shallow marine environment in the southeastern Tethys has changed to a suboxic–anoxic environment (Fig. 1).

On the other hand, the lack of V and U enrichments in the shallow marine sections of Kiritehere apparently does not indicate that these shallow depositional environments might have been oxygen-poor too. However, the

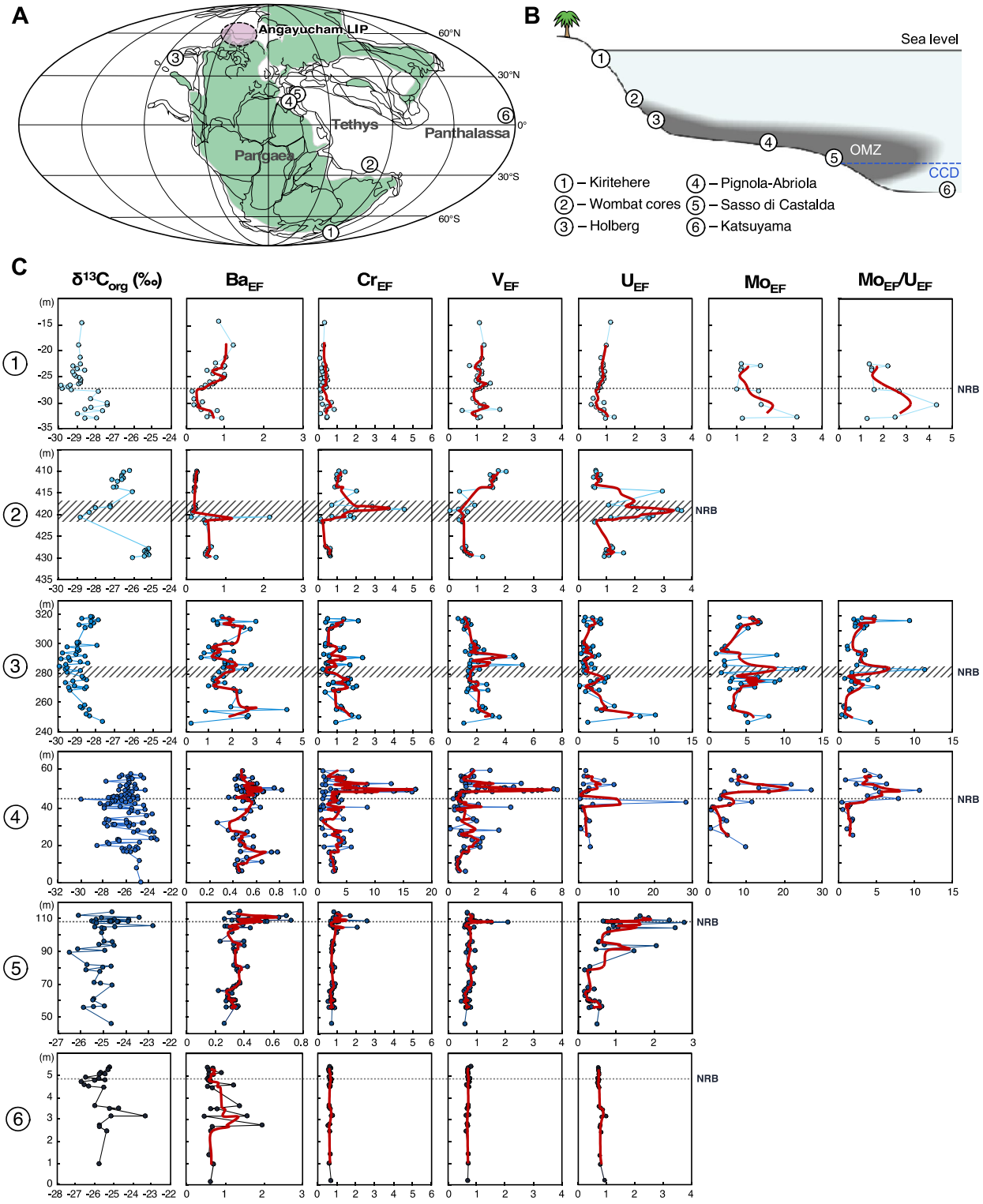

Figure 1. $\delta^{13}C_{org}$, Ba, and redox-sensitive elements (Mn, Cr, V, U, and Mo) show enrichments in the study sections. The stratigraphic position of the NRB is discussed in Supplementary Information. Blue dots represent raw data, and red lines show moving average on three samples.

Kiritehere section recorded the global extinction of pelagic and benthonic bivalves that belonged to the monitid group, so other mechanisms related to the spread of oxygen-deficient waters might be thus indicated (e.g., ocean acidification, competition, food shortage, eutrophication). In addition, no stratigraphic changes in concentrations of redox-sensitive elements were observed in the deep-sea pelagic deposits of Panthalassa, represented by the Katsuyama section. This suggests that the development of oxygen-poor conditions may not have extended to the deep seafloor of the mid-Panthalassic Ocean (Fig. 1).

Another common redox proxy for reducing conditions is the Mo_{EF}/U_{EF} ratio, which shows enrichment trends similar to those observed for V_{EF} in both the Pignola-Abriola and Holberg sections (Fig. 1). Covariations of Mo and U enrichment patterns (Fig. 2) and increased Mo_{EF}/U_{EF} ratios suggest the development of anoxic bottom water and scavenging of Mo by a Fe–Mn (oxyhydr)oxide particulate shuttle during the upper Sevatian to Rhaetian[38,49]. The occurrence of the particulate shuttle requires an oxic–anoxic redox boundary in the water column and rapid water replacement to maintain the predicted Fe–Mn redox behavior [38,50]. Thus, the Mo_{EF}/U_{EF} increase in the particulate shuttle field in the Holberg and Pignola-Abriola sections may indicate the development of intermediate-depth O_2 minima with redox boundaries on both sides of Pangea. However, Mo enrichment due to Mn- and Fe- particulate shuttles was less significant compared to modern sites with anoxic oxygen minimum zones (OMZs)[50]. Consequently, V enrichment and U_{EF} and Mo_{EF} trends suggest that anoxic conditions occurred in mid- to deep-water environments over a large area around Pangaea (Fig. 1).

Mo is a conservative hexavalent oxyanion (MoO_4^{2-}) in oxygenated water. The largest sink of Mo in the modern ocean (50%) is adsorption to manganese oxides, which preferentially retains light isotopes. This also occurs in MnO_2 formed on land. Reporting Mo isotope compositions and correcting published data sets to the NIST 3134 reference solution ($\delta^{98}Mo = (({}^{98}Mo/{}^{95}Mo)_{sample}/({}^{98}Mo/{}^{95}Mo)_{3134}-1)\times 1000$)[51], river water $\delta^{98}Mo$ averages + 0.54‰[52] and seawater + 2.09‰ ± 0.10[51], higher than the average continental crust based on molybdenite (0.04‰ ± 1.04) [53] or silicate rocks (+ 0.15‰)[54]. As the size of the marine Mn oxide sink of Mo changes over time, depending on the extent of anoxic basins, the $\delta^{98}Mo$ composition of seawater is expected to also change over time. For example, prior to OAE-2 at 94 Ma, seawater $\delta^{98}Mo$ was lower (+ 1.65‰)[55]. In conditions where free dissolved sulfide exists at concentrations exceeding 10 mM, Mo is quantitatively removed, and underlying sediments can preserve the isotopic composition of Mo in seawater. Today, euxinic basins are restricted to isolated systems like the Black Sea and fjords where exchange with the open ocean is poor, but in the past they may have been more common. In anoxic but non-euxinic basins, the isotope composition of sedimentary Mo depends on the presence or absence of Mn-oxides and bottom water oxygen. If porewater sulfide is sufficiently close to the sediment–water interface, while bottom water may not be euxinic, seawater Mo can diffuse into the sediment to give them a similar $\delta^{98}Mo$ to seawater, but the Mo concentration will be lower than in truly euxinic basins[57]. With slightly higher O_2 in bottom water, but with anoxic pore water, Mn-oxides with low $\delta^{98}Mo$ that formed within seawater can dissolve in the anoxic sediments, releasing their Mo with low $\delta^{98}Mo$. This Mo can diffuse up towards the seawater-sediment interface, or down where it can be trapped permanently in deeper, sulfidic sediments. Today, sediment $\delta^{98}Mo$ can range from ~ -1‰ in fully oxic systems to + 2.0‰ in euxinic systems, with intermediate values corresponding to redox state and the presence of sulfide. While modern ooids have a composition close to the seawater they precipitate from, use of skeletal carbonates ($\delta^{98}Mo_{carb}$) as a proxy of seawater can be affected by non-equilibrium (biological) fractionation. Furthermore, $\delta^{98}Mo$ of impure carbonates will also reflect contributions from detritus and Fe–Mn oxides, which is much lower than the seawater value.

Samples analysed for Mo isotopes were either carbonate-absent (CaO < 1%) or carbonate-bearing. The Mo in carbonate-absent sediments is derived from detritus or authigenic phases, namely Fe–Mn hydroxide and sulfides, while he carbonate-bearing samples also contain significant amounts of potentially isotopically distinct carbonate. Analyses were made on bulk samples, but to address the isotope composition of seawater derived phases, correction for detrital material is made. This is done by assuming all Ti is detrital, and using the upper continental crust (UCC) Mo/Ti composition to determine the amount of detritus-bound Mo. The isotope composition of the UCC is assumed to represent the detrital material, and for this we use UCC Mo concentrations and isotope composition of 1.1 ppm and + 0.1‰[58,59] to subtract the detrital contribution to the whole rock data by isotope mass balance, leaving a $\delta^{98}Mo$ value for authigenic (Fe–Mn hydroxide or sulfide) plus carbonate phases. The highest $\delta^{98}Mo$ in carbonate will be close to seawater, and our highest $\delta^{98}Mo_{carb}$ of + 1.65 is similar to that of Cretaceous seawater suggesting that Late Triassic seawater was somewhat similar[55]. In the

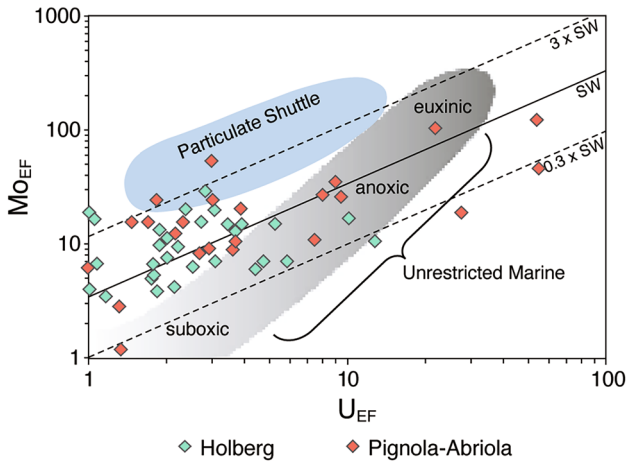

Figure 2. U_{EF} vs. Mo_{EF} diagram for samples in the study sections. Base figure modified from Algeo and Tribovillard[38].

Pignola-Abriola section, the $\delta^{98}Mo$ in carbonate-absent samples increases from -3.5‰ at 30 m to just 0.1‰ at 42.9 m, while the $\delta^{98}Mo$ in carbonate-bearing samples are more variable (-2.7‰ to + 1.7‰) (Fig. 3).

In an oxic water column, Fe–Mn hydroxides are 3‰ lower in $\delta^{98}Mo$ than seawater[56], but the lowest values of $\delta^{98}Mo$ we measure are more than 3‰ lower than our estimate of seawater at the time of formation. To increase this difference beyond 3‰, dissolution of Fe–Mn hydroxides (bearing low $\delta^{98}Mo$ signatures) followed by their re-oxidation is indicated, suggesting that the oxygen content of water close to the seawater sediment interface fluctuated in response to physical restriction, which is unlikely given the paleo-reconstruction of the Pignola-Abriola area, or to changes in the delivery of organic matter, supported by the correspondence between the lowest $\delta^{98}Mo$ and highest TOC%. The increase in $\delta^{98}Mo_{auth}$ from values consistent with a mostly, albeit variable, oxic water column to values consistent with anoxic to euxinic sediments underlying an expanding area of high productivity with a persistent oxygen minimum zone[61]. The increase in $\delta^{98}Mo_{auth}$ towards that of contemporaneous seawater indicated by the highest $\delta^{98}Mo_{carb}$ as Mo_{EF}/U_{EF} also increases supports the concept of intensification of an OMZ driven by increasing productivity, and the progression of a porewater sulfide front towards the sediment–seawater interface.

Possible cause(s)

These environmental perturbations can be explained by various mechanisms, any of which may create a global record, such as dissociation of clathrate hydrate and/or enhanced magmatic activity and outgassing[1,62,63]. Likely, a large volume of ^{13}C-depleted CO_2 entered the ocean–atmosphere system prior to the NRB, possibly as a product of volcanic outgassing by the emplacement of the Angayucham LIP[11,21,24,32,64]. This hypothesis is supported by the comparison of C-isotope records from marine[11] and terrestrial settings[21,22] with the seawater Sr-isotope[65] and Os-isotope curves[66–68]. The $^{87}Sr/^{86}Sr$ and $^{187}Os/^{188}Os$ values started to decline in the upper Norian, indicating a relative increase in the supply of mantle-derived unradiogenic Sr and Os from marine hydrothermal or other mafic igneous sources. Furthermore, the mechanism invoked to explain the spread of reducing conditions also implies significant input of CO_2 into the ocean–atmosphere system that would enhance chemical weathering via acceleration of the hydrological cycle during radiative-forced warming and cause increased nutrient discharge (e.g., nitrates and phosphates) to the global ocean[1,69,70]. The coincidence of these three concatenated steps has been clearly documented worldwide. Our weathering proxy data (Chemical Index of Alteration—CIA, Rb_{EF}, and K_{EF} values) have revealed that chemical weathering intensified during the development of anoxic conditions (Figs. 3, 4).

Values of the CIA from the shale samples[71] indicate the extent of decomposition of feldspar minerals, which are the most abundant mineral group in the UCC. Because of the high carbonate content of the study section, we used a modified form of the CIA equation by[33] as:

$$CIA^{*} = Al_2O_3/(Al_2O_3 + Na_2O + K_2O)/100,$$

CIA values are relatively constant below the FO level of *M. posthernsteini* s.l. sensu[34], and then rapidly increase in the S3 interval (sensu[32], Fig. 3). These stratigraphic variations in CIA values indicate intensified chemical weathering on continents during the S3 interval, implying that the climate changed to relatively warm and humid conditions. K and Rb were released from primary minerals, possibly micas and feldspars in felsic rocks, during continental chemical weathering. The stratigraphic variations in K_{EF} and Rb_{EF} decrease across the NRB, associated with a rapid increase in CIA values (Figs. 3, 4), which suggest the intensity of aluminosilicate chemical weathering increased during the anoxic event.

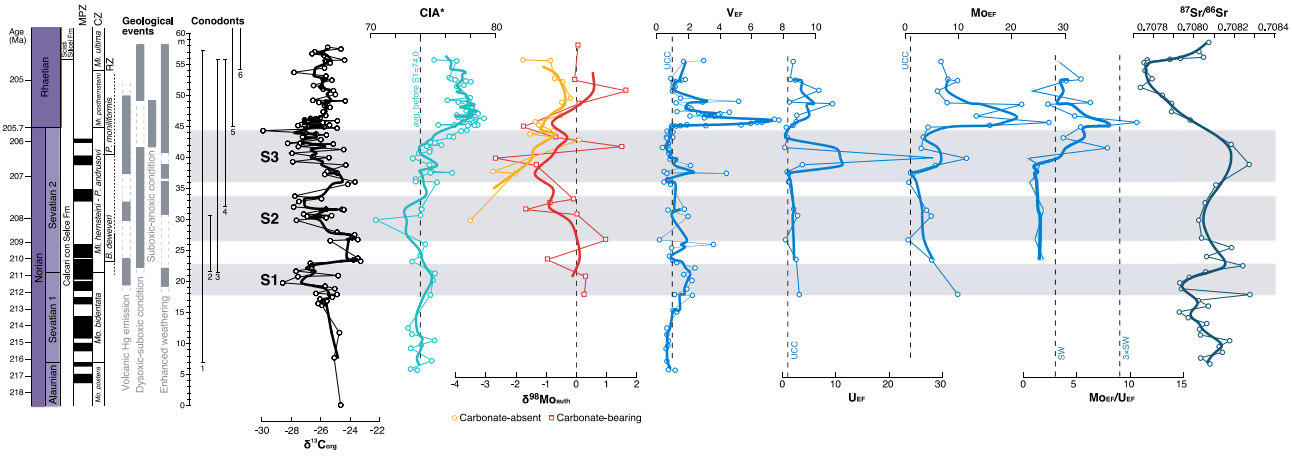

Figure 3. Geochemical profile of Pignola-Abriola section. Enrichment factors (EF) were calculated relative to UCC[58,60]. $\delta^{98}Mo_{auth}$ for carbonate-absent is of Fe–Mn hydroxides and for carbonate-bearing is Fe–Mn hydroxides plus carbonate. Strontium curve modified after[64]. A description of the taxonomic range of conodonts is as follows: 1. *Mockina bidentata*; 2. *Parvigondolella andrusovi*; 3. *Misikella hernsteini*; 4. *Mi. hernsteini/posthernsteini*; 5. *Mi. posthernsteini;* 6. *Mi. ultima*.

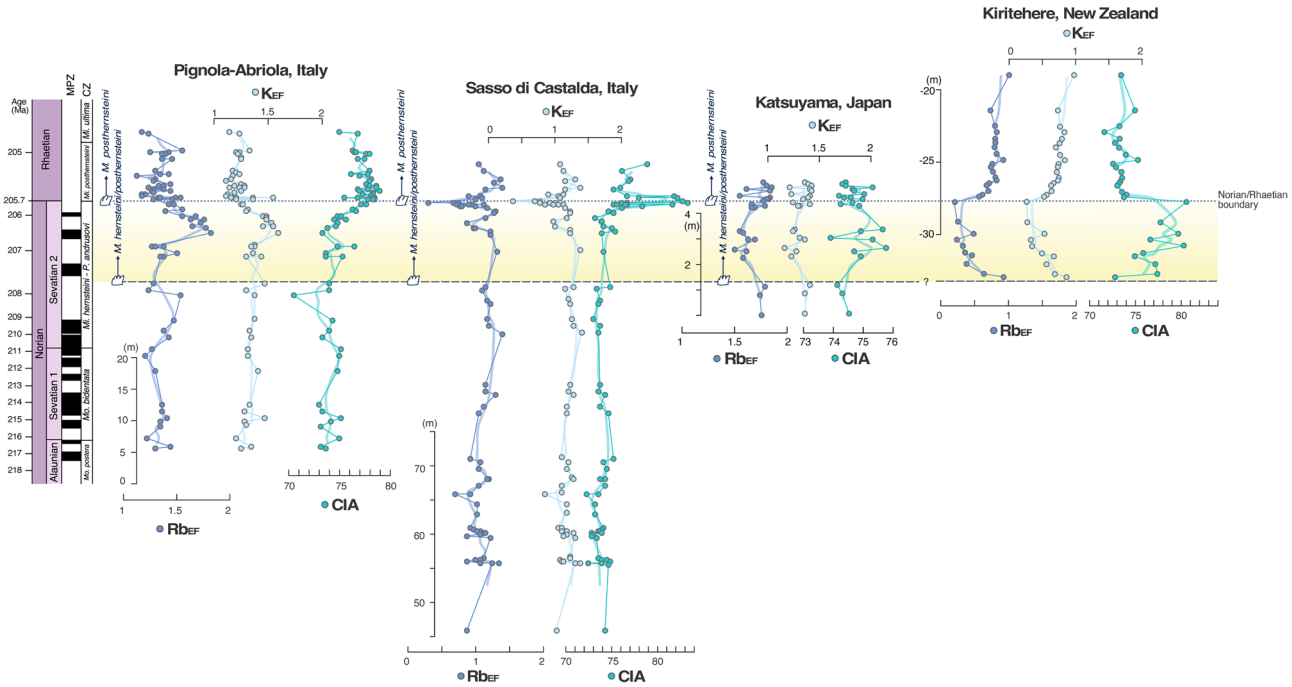

Figure 4. Stratigraphic profiles of K_{EF}, Rb_{EF}, and CIA in the Pignola-Abriola section. Enrichment factors (EF) were calculated relative to UCC[60]. K_{EF} and Rb_{EF} decrease with increasing CIA values across the NRB.

In theory, enhanced chemical weathering via acceleration of the hydrological cycle would cause increased nutrient discharge to the global ocean, with a consequent increase in biological productivity[1,70,72]. Barium is commonly used as a tracer of paleo-productivity[73–76], because barite precipitation occurs in decaying particulate organic matter while it sinks to the seafloor[74,77,78], which is supported by enhanced Ba_{EF} values below high-productivity areas[79]. Our data show that Ba_{EF} increased in the NRB, except in the Panthalassic Katsuyama section, deposited below the CCD (Fig. 1). Hence, our geochemical proxies show an apparent link between the volcanic event and oceanic anoxia via increased chemical weathering and paleo-productivity during the S3 interval.

High CIA continues after the boundary, indicating the persistence on land of the conditions that triggered the OAE even as the ocean began to recover, first exhibited by Mo_{EF}/U_{EF}[50]. $\delta^{98}Mo_{auth}$ also begins to record increasing oxic conditions well after the boundary, showing the control that Mn has on $\delta^{98}Mo$. The prolonged chemical weathering could be the result of a million-year timescale required for silicate weathering to consume the massive amounts of CO_2 emitted during volcanism. Long-term increases in CIA similar to the NRB have also been reported from the early Late Triassic Carnian Pluvial Episode (CPE; 232–234 Ma) and from the Triassic-Jurassic boundary[80,81]. In the case of the Triassic-Jurassic boundary, it is estimated that 1–2 myr were necessary for chemical weathering[80] to consume the large amount of CO_2 released by 600 kyr of volcanic activity[82]. CO_2 emissions from voluminous, pulsed volcanic activity across the NRB may have thus caused prolonged continental weathering in the Rhaetian.

In summary, our data document a previously unknown OAE of global extent, similar in nature to other OAEs. The OAE that spanned the NRB extended across the Panthalassa Ocean to both sides of the Pangea supercontinent and it is recorded in both the Northern and Southern Hemispheres, at different latitudes. As is the case for most OAEs, we propose that this Norian-Rhaetian oceanic oxygen depletion event resulted from large-volume emissions of volcanogenic greenhouse gases that accelerated the hydrological cycle, thereby increasing weathering rates and increasing nutrient delivery to the oceans. The increased nutrient supply enhanced primary productivity and export of organic carbon, resulting in oxygen depletion and expansion of the OMZ, which in turn increased the burial efficiency of organic carbon in sediments. Fossil extinctions and reducing conditions were documented in basins around the world (Italy, Canada, NW Australia, New Zealand), leaving an unmistakable record of the NRB OAE. The onset of the stepwise Late Triassic extinctions coincided with the NRB OAE, indicating that the combined climate and environmental changes impacted biota at this time. The trigger of this event is attributed to a volcanic event pre-dating the NRB or an alternative source of volcanogenic gas emissions, likely from the Angayucham LIP.

Data availability

All data generated or analyzed during this study are included in this published article and supplementary information files.

Received: 1 February 2024; Accepted: 1 July 2024
Published online: 06 July 2024

References

1. Jenkyns, H. C. Geochemistry of oceanic anoxic events. *Geochem. Geophys. Geosyst.* https://doi.org/10.1029/2009GC002788 (2010).
2. Schlanger, S.O. & Jenkyns, H. Cretaceous Oceanic Anoxic Events: Causes and consequences. Geologie en Mijnbouw **55**, 79–184 (1976).
3. Olsen, P. E. Giant Lava Flows, Mass Extinctions, and Mantle Plumes. *Science* **284**, 604–605 (1999).
4. Rampino, M. R. & Stothers, R. B. Flood Basalt Volcanism During the Past 250 Million Years. *Science* **241**, 663–668 (1988).
5. Reershemius, T. & PlanavskyN, J. What controls the duration and intensity of ocean anoxic events in the Paleozoic and the Mesozoic?. *Earth-Sci. Rev.* **221**, 103787 (2021).
6. Speijer, R. P. & Wagner, T. Sea-level changes and black shales associated with the late Paleocene thermal maximum: organic–geochemical and micropaleontologic evidence from the southern Tethyan margin (Egypt–Israel). *Geol. Soc. Am. Special Paper* **356**, 533–549 (2002).
7. Kump, L. R. & Arthur, M. A. Interpreting carbon-isotope excursions: carbonates and organic matter. *Chem. Geol.* **161**, 181–198 (1999).
8. Wignall, P. B. *et al.* An 80 million year oceanic redox history from Permian to Jurassic pelagic sediments of the Mino-Tamba terrane, SW Japan, and the origin of four mass extinctions. *Glob. Planetary Change* **7**, 109–123 (2010).
9. Padden, M. *et al.* Evidence for Late Jurassic release of methane from gas hydrate. *Geology* **29**, 223–226 (2001).
10. Pálfy, J. Z. & Smith, P. L. Synchrony between Early Jurassic extinction, oceanic anoxic event, and the Karoo-Ferrar flood basalt volcanism. *Geology* **28**, 747–750 (2000).
11. Rigo, M. *et al.* The Late Triassic Extinction at the Norian/Rhaetian boundary: Biotic evidence and geochemical signature. *Earth-Sci. Rev.* **204**, 103180 (2020).
12. McRoberts, C. A. *et al.* Thaetian (Late Triassic) *Monotis* (bivalvia: pectinoida) from the eastern Northern Calcareous Alps (Austria) and the end-Norian crisis in pelagic faunas. *Palaeontology* **51**, 721–735 (2008).
13. Todaro, S. *et al.* The end-Triassic mass extinction: A new correlation between extinction events and $\delta^{13}C$ fluctuations from a Triassic-Jurassic peritidal succession in western Sicily. *Sediment. Geol.* **368**, 105–113 (2018).
14. Lucas, S. G. Late Triassic Ammonoids: Distribution, Biostratigraphy and Biotic Events. In *The Late Triassic World: Earth in a Time of Transition* (ed. Tanner, L. H.) 237–261 (Springer International Publishing, 2018).
15. Whiteside, J. H. & Ward, P. D. Ammonoid diversity and disparity track episodes of chaotic carbon cycling during the early Mesozoic. *Geology* **39**, 99–102 (2011).
16. Carter, E. S. Late Triassic radiolarian biostratigraphy of the Kunga Group Queen Charlotte Islands, British Columbia. *Evol. Hydrocar. Potent. Queen Charlotte Basin Br. Columbia Geol. Survey Canada* **90**, 195–201 (1991).
17. Karádi, V. *et al.* The last phase of conodont evolution during the Late Triassic: Integrating biostratigraphic and phylogenetic approaches. *Palaeogeogr. Palaeoclimatol. Palaeoecol.* **549**, 109144 (2020).
18. O'Dogherty, L. *et al.* Triassic radiolarian biostratigraphy. In *The Triassic Timescale* (ed. Lucas, S. G.) 163–200 (Geological Society, 2010).
19. Renesto, S. & Dalla Vecchia, F.M. Late Triassic Marine Reptiles. In *The Late Triassic World: Earth in a Time of Transition* (ed. Tanner, L. H.) 263–313 (Springer International Publishing, 2018).
20. Stanley, G. D. The evolution of modern corals and their early history. *Earth-Sci. Rev.* **60**, 195–225 (2003).
21. Jin, X. *et al.* Terrestrial record of carbon-isotope shifts across the Norian/Rhaetian boundary: A high-resolution study from northwestern Sichuan Basin South China. *Glob. Planetary Change* **210**, 103754 (2022).
22. Fang, Y. *et al.* A possible Norian-Rhaetian boundary in the high-latitude continental Junggar Basin indicated by the δ13Corg record. *Geological Society, London, Special Publications* **538**, 67 (2024).
23. Bertinelli, A. *et al.* Stratigraphic evolution of the Triassic-Jurassic Sasso di Castalda succession (Lagonegro Basin, Southern Apennines, Italy). *Bollettino Della Società Geologica Italiana* **124**, 161–175 (2005).
24. Rigo, M. *et al.* The Pignola-Abriola section (southern Apennines, Italy): A new GSSP candidate for the base of the Rhaetian Stage. *Lethaia* **49**, 287–306 (2016).
25. Rigo, M. *et al.* Stratigraphy of the Carnian - Norian Calcari Con Selce Formation in the Lagonegro Basin, Southern Apennines. *Rivista Italiana di Paleontologia e Stratigrafia* **118**, 143–154 (2012).
26. Reggiani, L. *et al.* Triassic-Jurassic stratigraphy of the Madonna del Sirino succession (Lagonegro Basin, Southern Apennines, Italy). *Bollettino Della Società Geologica Italiana* **124**, 281–291 (2005).
27. Preto, N. *et al.* The calcareous nannofossil Prinsiosphaera achieved rock-forming abundances in the latest Triassic of western Tethys: consequences for the $\delta^{13}C$ of bulk carbonate. *Biogeosciences* **10**, 6053–6068 (2013).
28. Bazzucchi, P. *et al.* The Late Triassic-Jurassic stratigraphic succession of Pignola (Lagonegro- Molise Basin, Southern Apennines, Italy). *Boll. Soc. Geol. It.* **124**, 143–153 (2005).
29. Rigo, M. *et al.* Biostratigraphy of the Calcari con Selce formation. *Boll. Soc. Geol. Ital.* **124**, 293–300 (2005).
30. Sato, H. *et al.* Sedimentary record of Upper Triassic impact in the Lagonegro Basin, southern Italy: Insights from highly siderophile elements and Re-Os isotope stratigraphy across the Norian/Rhaetian boundary. *Chem. Geol.* **586**, 120506 (2021).
31. Maron, M. *et al.* Weathering trends in the Norian through geochemical and rock magnetic analyses from the Pignola-Abriola Section (Lagonegro Basin, Italy). *Clim. Past* **20**, 637–658 (2024).
32. Zaffani, M. *et al.* The Norian "chaotic carbon interval": New clues from the delta C-13(org) record of the Lagonegro Basin (southern Italy). *Geosphere* **13**, 1133–1148 (2017).
33. Casacci, M. *et al.* Carbonate-to-biosilica transition at the Norian-Rhaetian boundary controlled by rift-related subsidence in the western Tethyan Lagonegro Basin (southern Italy). *Palaeogeogr. Palaeoclimatol. Palaeoecol.* **456**, 21–36 (2016).
34. Bertinelli, A. *et al.* The Norian/Rhaetian boundary interval at Pignola-Abriola section (southern Apennines, Italy) as a GSSP candidate for the Rhaetian stage: an update. *Albertiana* **43**, 5–18 (2016).
35. Maron, M. *et al.* Magnetostratigraphy, biostratigraphy, and chemostratigraphy of the Pignola-Abriola section: New constraints for the Norian-Rhaetian boundary. *GSA Bull.* **127**, 962–974. https://doi.org/10.1130/B31106.1 (2015).
36. Gardin, S. *et al.* Where and when the earliest coccolithophores?. *Lethaia* **45**, 507–523 (2012).
37. Rigo, M. & Campbell, C. Correlation between the Warepan/Otapirian and the Norian/Rhaetian stage boundary: Implications of a global negative δ13Corg perturbation. *N. Zealand J. Geol. Geophys.* **65**, 397–406 (2022).
38. Algeo, T. J. & Tribovillard, N. Environmental analysis of paleoceanographic systems based on molybdenum-uranium covariation. *Chem. Geol.* **268**, 211–225 (2009).
39. Fujisaki, W. *et al.* Tracking the redox history and nitrogen cycle in the pelagic Panthalassic deep ocean in the Middle Triassic to Early Jurassic: Insights from redox-sensitive elements and nitrogen isotopes. *Palaeogeogr. Palaeoclimatol. Palaeoecol.* **449**, 397–420 (2016).
40. Sato, H. *et al.* Biotic and environmental changes in the Panthalassa Ocean across the Norian (late Triassic) impact event. *Prog. Earth Planet. Sci.* **7**, 61 (2020).
41. Soda, K. & Onoue, T. Multivariate analysis of geochemical compositions of bedded chert during the Middle Triassic (Anisian) oceanic anoxic events in the Panthalassic Ocean. *Geochem. J.* **53**, 91–102 (2019).
42. Tomimatsu, Y. *et al.* Pelagic responses to oceanic anoxia during the Carnian Pluvial Episode (Late Triassic) in Panthalassa Ocean. *Sci. Rep.* **13**, 16316 (2023).

43. Calvert, S. E. & Pedersen, T. F. Geochemistry of Recent oxic and anoxic marine sediments: Implications for the geological record. *Marine Geol.* **113**, 67–88 (1993).
44. Calvert, S. E. & Pedersen, T. F. Elemental proxies for palaeoclimatic and palaeoceanographic variability in marine sediments. In *Developments in Marine Geology* (ed. Hillaire-Marcel, C.) (Elsevier, 2007).
45. Algeo, T. J. & Li, C. Redox classification and calibration of redox thresholds in sedimentary systems. *Geochim. Cosmochim. Acta* **287**, 8–26 (2020).
46. Onoue, T., Soda, K. & Isozaki, Y. Development of deep-sea anoxia in Panthalassa during the Lopingian (late Permian): Insights from redox-sensitive elements and multivariate analysis. *Front. Earth Sci.* **8**, 685 (2021).
47. Tyson, R. & Pearson, T. Modern and ancient continental shelf anoxia: an overview. *Geol. Soc. Sepc. Publ.* **58**, 1–24. https://doi.org/10.1144/GSL.SP.1991.058.01.01 (1991).
48. Wanty, R. B. & Goldhaber, M. B. Thermodynamics and kinetics of reactions involving vanadium in natural systems: Accumulation of vanadium in sedimentary rocks. *Geochimica Cosmochimica Acta* **56**, 1471–1483 (1992).
49. Tribovillard, N., Algeo, T. J., Baudin, F. & Riboulleau, A. Analysis of marine environmental conditions based on molybdenum-uranium covariation-Applications to Mesozoic paleoceanography. *Chem. Geol.* **324**, 46–58 (2012).
50. Scholz, F., McManus, J. & Sommer, S. The manganese and iron shuttle in a modern euxinic basin and implications for molybdenum cycling at euxinic ocean margins. *Chem. Geol.* **355**, 56–68 (2013).
51. Goldberg, T. *et al.* Resolution of inter-laboratory discrepancies in Mo isotope data: An intercalibration. *J. Anal. Atomic Spectr.* **28**, 724–735 (2013).
52. Archer, C. & Vance, D. The isotopic signature of the global riverine molybdenum flux and anoxia in the ancient oceans. *Nat. Geosci.* **1**, 597–600 (2008).
53. Breillat, N., Guerrot, C., Marcoux, E. & Négrel, P. A new global database of δ^{98}Mo in molybdenites: A literature review and new data. *J. Geochem. Expl.* **161**, 1–15 (2014).
54. Willbold, M. & Elliott, T. Molybdenum isotope variatons in magmatic rocks. *Chem. Geol.* **449**, 253–268 (2017).
55. Siebert, C., Scholz, F. & Kuhnt, W. A new view on the evolution of seawater molybdenum inventories before and during the Cretaceous Oceanic Anoxic Event 2. *Chem. Geol.* **582**, 120399 (2021).
56. Siebert, C., Nägler, T. F., von Blanckenburg, F. & Kramers, J. D. Molybdenum isotope records as a potential new proxy for paleoceanography. *Earth Planetary Sci. Lett.* **211**, 159–171 (2003).
57. Scott, C. & Lyons, T. W. Contrasting Molybdenum Cycling and Isotopic Properties in Euxinic versus Non-Euxinic Sediments and Sedimentary Rocks: Refining the Paleoproxies. *Chem. Geol.* **324–325**, 19–27 (2012).
58. Rudnick, R. & Gao, S. Composition of the continental crust. In *Treatise on Geochemistry* (ed. Rudnick, R. L.) 1–64 (Elsevier - Pergamon, 2014).
59. Bezard, R. & Guo, H. Fluid-melt Mo isotope fractionation: implications for the $\delta^{98/95}$Mo of the upper crust. *Geochemical Perspectives Letters* **26**, 25–30 (2023).
60. McLennan, S.M. Relationships between the trace element composition of sedimentary rocks and upper continental crust. *Geochem. Geophys. Geosyst.* **2**, 2000GC000109 (2001).
61. He, Z. *et al.* Temporally and spatially dynamic redox conditions on an upwelling margin: The impact on coupled sedimentary Mo and U isotope systematics, and implications for the Mo-U paleoredox proxy. *Geochimica Cosmochimica Acta* **309**, 251–271 (2021).
62. Korte, C., Kozur, H. W., Bruckschen, P. & Veizer, J. Strontium isotope evolution of Late Permian and Triassic seawater. *Geochimica et Cosmochimica Acta* **67**, 47–62 (2003).
63. Meyers, P. A. Why are the δ13Corg values in Phanerozoic black shales more negative than in modern marine organic matter?. *Geochem. Geophys. Geosyst.* **15**, 3085–3106 (2014).
64. Jin, X. *et al.* Carbon-isotope excursions in the Norian stage (Upper Triassic) of the Baoshan terrane, western Yunnan. *China. J. Asian Earth Sci.* **230**, 105215 (2022).
65. Callegaro, S., Rigo, M., Chiaradia, M. & Marzoli, A. Latest Triassic marine Sr isotopic variations, possible causes and implications. *Terra Nova* **24**, 130–135 (2012).
66. Kuroda, J., Hori, R. S., Suzuki, K., Gröcke, D. R. & Ohkouchi, N. Marine osmium isotope record across the Triassic-Jurassic boundary from a Pacific pelagic site. *Geology* **38**, 1095–1098 (2010).
67. Nozaki, T. *et al.* Triassic marine Os isotope record from a pelagic chert succession, Sakahogi section, Mino Belt, southwest Japan. *J. Asian Earth Sci.* **10**, 100004 (2019).
68. Sato, H. *et al.* Rhenium-osmium isotope evidence for the onset of volcanism in the central Panthalassa Ocean during the Norian "chaotic carbon episode". *Glob. Planetary Change* **229**, 104239 (2023).
69. Pearce, C. R., Cohen, A. S., Coe, A. L. & Burton, K. W. Molybdenum isotope evidence for global ocean anoxia coupled with perturbations to the carbon cycle during the Early Jurassic. *Geology* **36**, 231–234 (2008).
70. Pogge von Strandmann, P. A. E., Jenkyns, H. C. & Woodfine, R. G. Lithium isotope evidence for enhanced weathering during Oceanic Anoxic Event 2. *Nat. Geosci.* **6**, 668–672 (2013).
71. Nesbitt, H. W. & Young, G. M. Early Proterozoic Climates and Plate Motions Inferred from Major Element Chemistry of Lutites. *Nature* **299**(5885), 715–717 (1982).
72. Jones, C. E. & Jenkyns, H. C. Seawater strontium isotopes, oceanic anoxic events, and seafloor hydrothermal activity in the Jurassic and Cretaceous. *Am. J. Sci.* **301**, 112–149 (2001).
73. Zachos, J. C., Arthur, M. A. & Dean, W. E. Geochemical evidence for suppression of pelagic marine productivity at the cretaceous tertiary boundary. *Nature* **337**(6202), 61–64 (1989).
74. Dymond, J. & Collier, R. Particulate barium fluxes and their relationships to biological productivity. *Deep Sea Res. Part II Topical Stud. Oceanogr.* **43**, 1283–1308 (1996).
75. McManus, J. *et al.* Geochemistry of barium in marine sediments: implications for its use as a paleoproxy. *Geochimica Cosmochimica Acta* **62**, 3453–3473 (1998).
76. Algeo, T. J. *et al.* Spatial variation in sediment fluxes, redox conditions, and productivity in the Permian-Triassic Panthalassic Ocean. *Palaeogeogr. Palaeoclimatol. Palaeoecol.* **308**, 65–83 (2011).
77. Dehairs, F., Chesselet, R. & Jedwab, J. Discrete suspended particles of barite and the barium cycle in the open ocean. *Earth and Planetary Science Letters* **49**, 528–550 (1980).
78. Bishop, J. K. B. The barite-opal-organic carbon association in oceanic particulate matter. *Nature* **332**, 341–343 (1988).
79. Nürnberg, C. C., Bohrmann, G., Schlüter, M. & Frank, M. Barium accumulation in the Atlantic sector of the Southern Ocean: Results From 190,000-year records. *Paleoceanography* **12**, 594–603 (1997).
80. Shen, J. *et al.* Intensified continental chemical weathering and carbon-cycle perturbations linked to volcanism during the Triassic-Jurassic transition. *Nature Communications* **13**, 299 (2022).
81. Pecorari, M. *et al.* Weathering and sea level control on siliciclastic deposition during the Carnian Pluvial Episode (Southern Alps, Italy). *Palaeogeogr. Palaeoclimatol. Palaeoecol.* **617**, 111495 (2023).
82. Davies, J. H. F. L. *et al.* End-Triassic mass extinction started by intrusive CAMP activity. *Nat. Commun.* **8**, 15596 (2017).

Acknowledgements
This research used also samples provided by the Ocean Discovery Program (ODP, Site 761C), assisted by Dr. L. Gupta (IODP Curator, Kochi Core Center—KCC), who is warmly thanked; thanks to A. Thibodeau for deep discussion about geochemical proxies. We would like to thank the Editor A. Ferretti and two anonymous referees who constructively reviewed this manuscript.

Author contributions
MR developed the hypothesis and conceived the study with TO, XJ, LG, MEK, HS, YT and MZ and wrote the manuscript. MR, MZ, LG and MEK analyzed carbon isotopes from organic matter; GC and AC run TOC analyses. TO, HS, YT and MR analysed and interpreted the geochemical data and contributed to writing the manuscript. LG provided Mo analyses, interpretation and wrote the manuscript. QW, YD, JZXL, CSvW, LT, HC and AB provided advice and comments on the manuscript. Field work by MR, TO, MM, HS, YT, LT, JZXL, HC and AB.

Funding
This study was supported by the PRIN 2017W2MARE by the Italian MUR (Ministero dell'Università e della Ricerca) to M. Rigo and S. Satolli, and by PRIN PNRR P2022K9BE8 to M. Rigo; and by the Japan Society for the Promotion of Science, grants 16KK0104, 17H02975, JP20H00203 to T. Onoue and JP20K04113 to H. Sato.

Competing interests
The authors declare no competing interests.

Additional information
Supplementary Information The online version contains supplementary material available at https://doi.org/10.1038/s41598-024-66343-z.

Correspondence and requests for materials should be addressed to M.R.

Reprints and permissions information is available at www.nature.com/reprints.

Publisher's note Springer Nature remains neutral with regard to jurisdictional claims in published maps and institutional affiliations.